Effect of Cage Charges on Multiphoton Absorptions: First-Principles Study on Metallofullerenes $Sc_2C_2@C_{68}$ and $Sc_3N@C_{68}$

W.-D. Cheng,*,† H. Hu,† D.-S. Wu,‡ J.-Y. Wang,† S.-P. Huang,† Z. Xe,† and H. Zhang†

State Key Laboratory of Structural Chemistry, Fujian Institute of Research on the Structure of Matter, Chinese Academy of Sciences, Fuzhou, Fujian 350002, People's Republic of China, and Department of Chemical and Biomolecular Engineering, University of Tennessee, Knoxville, Tennessee 37996

Received: December 8, 2008; Revised Manuscript Received: March 17, 2009

A combined method of the time-dependent density functional theory (TDDFT) and sum-overstate (SOS) formula was implemented to model multiphoton absorption spectra, including two-photon absorption (2PA) and three-photon absorption (3PA), of $Sc_2C_2@C_{68}$ and $Sc_3N@C_{68}$ endohedral metallofullerenes (EMFs). This method has been proved to be effective by comparisons between the calculated and experimental results of *trans*-4,4′-bis[diphenylamino]stilbene. It was found that the multiphoton absorption cross sections were larger for $Sc_2C_2@C_{68}$ than that of $Sc_3N@C_{68}$. The electronic origin of multiphoton absorption has been identified with respect to the molecular orbitals involved in charge transfer process. It shows that the increase of π-charges on the cage of C_{68} results in a large multiphoton absorption cross section in EMFs.

1. Introduction

Since the late 1980s, multiphoton absorption has become a focused topic[1−4] in photophysics due to highly demanded applications, such as three-dimensional (3D) optical data storage and microfabrication,[5,6] photodynamic therapy and bioimaging,[7−11] optical power limiting,[12,13] etc.[14−16] In order to meet the requirements of actual applications, scientists have made great efforts to develop new materials with large two-photon absorption (2PA) and three-photon absorption (3PA) cross section. At the same time, it has become a subject of interest to understand the electronic origin of large 2PA and 3PA cross sections in materials. Recently, endohedral fullerenes have attracted more and more attention due to their unique structure-related properties and their potential applications in electronics and magnetism. The endohedral structure stabilizes the construction of pure carbon fullerenes in which pentagons do not obey the isolated-pentagon rule (IPR) that requires all pentagons to be surrounded by five hexagons.[17−19] Although endohedral metallofullerenes (EMFs) have been widely studied in various aspects, the nonlinear optical properties of EMFs having a non-IPR cage have not been reported to date.

In this work, we have employed time-dependent density functional theory (TDDFT) combined with the sum-overstate (SOS) method to model the 2PA and 3PA cross sections of $Sc_2C_2@C_{68}$ and $Sc_3N@C_{68}$ EMFs. The rational designs of molecules with multiphoton absorption properties were begun in 1990s with the aid of rapid increases in computer power, which allow us to undertake large-scale and accurate quantum mechanical calculations. The quantum mechanical analysis of multiphoton absorption demands highly correlated calculations at high-level theory. The accurate dipole polarizabilities from ab initio and DFT calculations have been evaluated by other groups considering the effect of different basis sets and levels of calculations.[20,21] Therefore, we applied TDDFT with 6-311G** basis sets for electronic structure calculations of $Sc_2C_2@C_{68}$ and $Sc_3N@C_{68}$ EMFs in the Gaussian 03 software package.[22,23] On the basis of the results from TDDFT calculations, 2PA and 3PA cross sections were then evaluated with our self-developed SOS code. By investigating the influences of cage charges on 2PA and 3PA cross sections, we will further identify the electronic origin of 2PA and 3PA for the studied EMFs. We expect that our theoretical model used in the current study could provide an economical way to search for innovated materials with large 2PA and 3PA cross sections.

2. Calculational Method and Procedures

The 2PA cross section δ can be related to the imaginary part of the third-order polarizability $\gamma(-\omega;\omega,\omega,-\omega)$ at degenerate four-wave mixing process as[24,25]

$$\delta(\omega) = \frac{8\pi^2\hbar\omega^2}{n^2c^2}L^4 \,\mathrm{Im}\,\gamma(-\omega;\omega,\omega,-\omega) \tag{1}$$

where $\hbar$ is Planck's constant divided by 2π, ω denotes the frequency of the perturbating radiation field, n is the refractive index, c is the speed of light in vacuum, and L is the local field factor (equal to 1 for vacuum). The frequency-dependent polarizability γ can be calculated by the SOS method as follows[26−30]

$$\gamma_{ijkl}(-\omega_{\mathrm{pol}};\omega_1,\omega_2,\omega_3) = (2\pi/h)^3 K(-\omega_{\mathrm{pol}};\omega_1,\omega_2,\omega_3)e^4 \sum_{\mathrm{perm}} \times \left[\sum_{m,n,p(\neq r)} \frac{\langle r|\mu_i|m\rangle\langle m|\bar{\mu}_j|n\rangle\langle n|\bar{\mu}_k|p\rangle\langle p|\mu_l|r\rangle}{(\omega_{mr}-\omega_{\mathrm{pol}}-i\Gamma_{mr})(\omega_{nr}-\omega_2-\omega_3-i\Gamma_{nr})\times(\omega_{pr}-\omega_3-i\Gamma_{pr})} - \sum_{m,n(\neq r)} \frac{\langle r|\mu_i|m\rangle\langle m|\mu_j|r\rangle\langle r|\mu_k|n\rangle\langle n|\mu_l|r\rangle}{(\omega_{mr}-\omega_{\mathrm{pol}}-i\Gamma_{mr})(\omega_{nr}-\omega_3-i\Gamma_{nr})\times(\omega_{nr}-\omega_2-i\Gamma_{nr})} \right] \tag{2}$$

where $\omega_{\mathrm{pol}} = \omega_1 + \omega_2 + \omega_3$ is the polarization response frequency, $K(-\omega_{\mathrm{pol}};\omega_1,\omega_2,\omega_3)$ is a numeric coefficient to match

† State Key Laboratory of Structural Chemistry, Fujian Institute of Research on the Structure of Matter, Chinese Academy of Sciences.

‡ Department of Chemical and Biomolecular Engineering, University of Tennessee.

10.1021/jp810806b CCC: $40.75 © 2009 American Chemical Society
Published on Web 04/29/2009

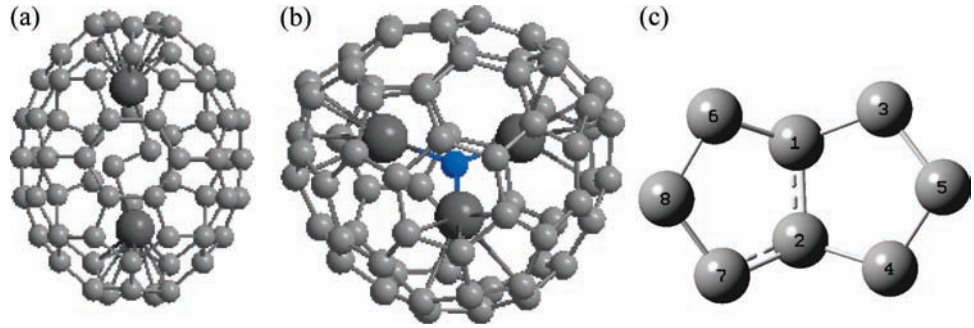

Figure 1. Molecular configurations of (a) $Sc_2C_2@C_{68}$ and (b) $Sc_3N@C_{68}$ and (c) labeling of carbon atoms on a pentagon−pentagon pair.

different optical processes, $\langle r|\mu_i|m\rangle$ is the electronic transition moment between the reference state r and excited state m along the ith Cartesian axis, $\langle m|\overline{\mu_j}|n\rangle$denotes the dipole difference operator equal to $\langle m|\mu_j|n\rangle - \langle r|\mu_j|r\rangle\delta_{mn}$, ω_{mr} is the transition energy between excited state m and the reference state r, and Γ_{mr} is damping associated with excited state m.

In a similar way concerning higher-order polarizations, the 3PA cross section σ can be derived from the imaginary part of the fifth-order polarizability $\varepsilon(-\omega;\omega,-\omega,\omega,-\omega,\omega)$. However, the numerical calculation of this polarizability through the full SOS approach is quite computational expensive.[31] With resonant condition considered, the 3PA cross section can be simplified as[32−34]

$$\sigma(\omega) = \frac{4\pi^2(\hbar\omega)^3}{\hbar^3 n^3 c^5} L^6 \sum_f |T^{ijk}_{g\to f}|^2 \left\{ \frac{\Gamma}{(E_{gf} - 3\hbar\omega)^2 + \Gamma^2} \right\} \tag{3}$$

where Γ is a Lorentzian broadening factor (set to 0.1 eV in the calculations), $T_{g\to f}$ corresponds to the three photon transition amplitude from the ground-state to a final three-photon state f, with tensor ijk elements given by

$$T^{ijk}_{g\to f} = P_{ijk} \sum_{m,n} \frac{\langle g|\mu_i|m\rangle\langle m|\mu_j|n\rangle\langle n|\mu_k|f\rangle}{(E_{gm} - \hbar\omega - i\Gamma)(E_{gn} - 2\hbar\omega - i\Gamma)} \tag{4}$$

The third-order transition moment has to be orientationally averaged as suggested by McClain.[35] For linearly and circularly polarized lights, the three-photon probabilities are given by

$$\sigma^{3PA}_L = \frac{1}{35}(3\sum_{ijk} T_{ijk}T_{ijk} + 2\sum_{ijk} T_{iij}T_{kkj}) \tag{5}$$

and

$$\sigma^{3PA}_C = \frac{1}{35}(5\sum_{ijk} T_{ijk}T_{ijk} - 2\sum_{ijk} T_{iij}T_{kkj}) \tag{6}$$

Before we make the calculations of 2PA and 3PA cross sections, the equilibrium geometrical structures of $Sc_2C_2@C_{68}$ and $Sc_3N@C_{68}$ were first optimized using the B3LYP method[36] at the 6-31G* level. Their state−state transition energies and transition moments were computed based on the optimized structures using TDDFT[37,38] at the B3LYP/6-311G** level and later used as the input for SOS calculations. It should be noted here that the ground-state electric dipole moment $\langle\Psi_g|\boldsymbol{\mu}|\Psi_g\rangle$ and transition moments from the ground-state to excited states $\langle\Psi_g|\boldsymbol{\mu}|\Psi_m\rangle$ can be directly obtained from the outputs of the TDDFT calculations. The excitation moments of $\langle\Psi_m|\boldsymbol{\mu}|\Psi_n\rangle$ are computed from the off-diagonal electric dipole matrix element ($m \neq n$, transition moment) and diagonal matrix element ($m = n$, dipole moment).

In our excited-state calculations, the core orbitals were frozen and the ranges of molecular orbitals in the correlation calculations were chosen from 89 to 1352 for $Sc_2C_2@C_{68}$ and 97 to 1380 for $Sc_3N@C_{68}$, respectively. The self-consistent field convergence criterions were set by the default values from Gaussian 03 program. The iterations were continued until the changes of the state energies were no more than 10^{-7} a.u. during the excited-state calculations. This resulted in the convergence of the first 50 excited states.

Due to the absence of experimental multiphoton absorption spectra of $Sc_2C_2@C_{68}$ and $Sc_3N@C_{68}$ EMFs, we calculate the 2PA and 3PA cross sections of *trans*-4,4′-bis[diphenylamino]stilbene (BDPAS) by the same method and compare the obtained results with the experimental data of BDPAS to test our method. Figure S1 in Supporting Information gives the plot of the wavelength-dependent 2PA cross section and shows that the 2PA cross section δ at input wavelength of 698 nm (peak position) is about 394 GM (1 GM = 10^{-50} cm^4 s). By comparing our calculated δ value with the measured ones of 190 and 320 GM using a two-photon-induced fluorescence method at laser wavelengths of 690 and 670 nm,[39,40] we verify that our calculated value is reasonable. Wavelength-dependent 3PA cross sections were also calculated and plotted in Figure S2 in Supporting Information. The calculated σ value from average linear polarization is about 1.09×10^{-80} cm^6 s^2, corresponding to the peak position at input wavelength of 1010 nm (1.23 eV). The measured 3PA cross section σ value is 0.50×10^{-80} cm^6 s^2 at a wavelength of 1175 nm (1.06 eV),[41,42] and the calculated values reported by other authors range from 0.667×10^{-80} to 22.8×10^{-80} cm^6 s^2 when using different theoretical methods.[33,43] The comparisons show that our calculated results are in good agreement with those from experiments and other calculations, and accordingly our calculation method is applicable for our further study on $Sc_2C_2@C_{68}$ and $Sc_3N@C_{68}$ EMFs.

3. Results and Discussion

3.1. Geometrical Structures. Figure 1 depicts the optimized configurations of $Sc_2C_2@C_{68}$ and $Sc_3N@C_{68}$ molecules. The carbon cages of C_{68} do not obey IPR, and they are stabilized by embedded molecule Sc_2C_2 or Sc_3N.[17,18] In the C_2 symmetrical $Sc_2C_2@C_{68}$, there are two pairs of pentagon−pentagon fusion sites in the C_{2v} symmetrical C_{68} parent, and the embedded Sc_2C_2 exists in a ladder structure in which each Sc atom coordinates with one pentagon−pentagon pair.[17] The calculated average Sc−C bond length (C on a pentagon−pentagon fusion site) is 2.358 Å. In the structures of $Sc_3N@C_{68}$ with D_3 symmetrical parent C_{68}, the embedded Sc_3N exists on a plane with each Sc atom coordinating to three pairs of pentagon−pentagon fusion sites,[18] respectively. The calculated average Sc−C bond length (C on a pentagon−pentagon fusion site) is 2.378 Å as compared with the experimental value of 2.336 Å for $Sc_3N@C_{68}$.[18] Table

TABLE 1: The Calculated Bond Lengths (Å) and Bond Angles (deg)

	$Sc_3N@C_{68}$			$Sc_2C_2@C_{68}$
	exptl[a]	PBE/DZVP[b]	B3LYP/6-31G*	B3LYP/6-31G*
Sc−C1	2.23	2.31	2.32	2.26
Sc−C2	2.28	2.31	2.32	2.29
Sc−C3	2.31	2.39	2.36	2.31
Sc−C4	2.35	2.35	2.39	2.38
Sc−C5	2.40	2.44	2.44	2.44
Sc−C6	2.30	2.35	2.39	2.38
Sc−C7	2.39	2.39	2.36	2.38
Sc−C8	2.43	2.44	2.44	2.42
C7C2C1C4	134.4	131.5	131.7	131.8

[a] Reference 18. [b] Reference 44.

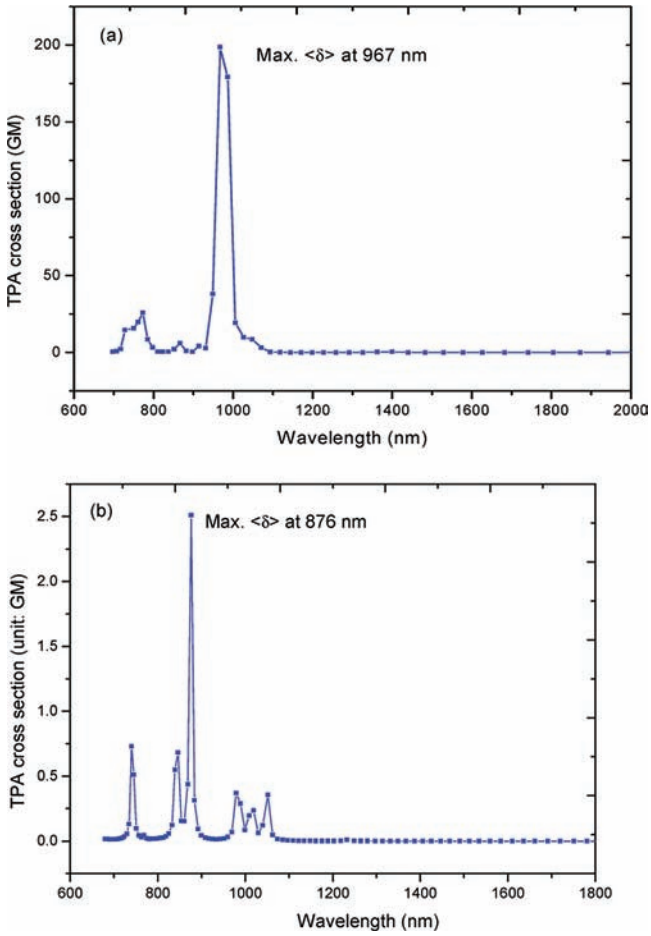

Figure 2. The wavelength-dependent two-photon absorption cross sections of (a) $Sc_2C_2@C_{68}$ and (b) $Sc_3N@C_{68}$.

1 lists some Sc−C bond lengths from theoretical calculations together with the available experimental data. It can be found that our calculated Sc−C bond lengths for $Sc_3N@C_{68}$ based on B3LYP/6-31G* generally agree well with the experimental data but also show some degrees of overestimation.

3.2. Two-Photon Absorption. Figure 2 shows the plots of the average wavelength-dependent 2PA cross sections $\langle\delta(\omega)\rangle$ for $Sc_2C_2@C_{68}$ and $Sc_3N@C_{68}$. The absorption peaks from $Sc_2C_2@C_{68}$ and $Sc_3N@C_{68}$, which correspond to the maximum of $\langle\delta(\omega)\rangle$, are located at wavelengths of about 967 and 876 nm, respectively. The absorption peak from $Sc_2C_2@C_{68}$ is a red-shift as compared with that from $Sc_3N@C_{68}$. The $\langle\delta(\omega)\rangle$ value (198.72 GM) of the EMF encased with a Sc_2C_2 molecule is much larger than that (2.51 GM) of EMF encased with a Sc_3N molecule in cage C_{68}. This interesting phenomenon can be understood from the second hyperpolarizabilities which make significant contribution to $\langle\delta(\omega)\rangle$ at a given wavelength. The calculations of hyperpolarizabilities by eq 2 require the input parameters of the corresponding dipole and transitions moments which are listed in Tables S1 and S2 in Supporting Information. As mentioned above, the $\delta(\omega)$ value only depends on the imaginary part of the second hyperpolarizability, Im $\gamma(-\omega;\omega,\omega,-\omega)$, at a specified input frequency. Accordingly, the two-photon states contributing to Im $\gamma(-\omega;\omega,\omega,-\omega)$ determine the $\delta(\omega)$ as well. Figure 3 gives the plots of average Im $\langle\gamma(-\omega;\omega,\omega,-\omega)\rangle$ value vs two-photon states at the characteristic wavelength (resonant wavelength). It can be found that only one two-photon resonant state, S_{19} (19th state) of $Sc_2C_2@C68$ and S_{22} (22nd state) of $Sc_3N@C_{68}$, makes a large contribution to Im $\langle\gamma(-\omega;\omega,\omega,-\omega)\rangle$. Analysis in terms of the configuration interactions shows that S_{19} of $Sc_2C_2@C_{68}$ is constructed by the configuration of $0.4125(MO_{223} \rightarrow MO_{232}) + 0.5267(MO_{227} \rightarrow MO_{233})$. Further analysis reveals that the occupied molecular orbital MO_{223} is contributed from Sc_2C_2 by 41.6% and MO_{227} is contributed from Sc_2C_2 by 1.76%. The unoccupied molecular orbitals MO_{232} and MO_{233} have contributions from Sc_2C_2 by 1.27% and 3.20%, respectively. For the $Sc_3N@C_{68}$, S_{22} is constructed from the configuration of $0.4598(MO_{237} \rightarrow MO_{245}) + 0.4598(MO_{238} \rightarrow MO_{246})$, in which the occupied molecular orbitals of both MO_{237} and MO_{238} are contributed from Sc_3N by 2% and C_{68} cage by 98%, while the unoccupied molecular orbitals of both MO_{245} and MO_{246} are contributions from Sc_3N by 13% and C_{68} cage by 87%. Figure 4 gives the plots of the molecular orbitals involved in the charge transfer processes corresponding to the configuration interaction described above. Parts a and b of Figure 4 show the orbitals contributing the most to the two-photon resonant state S_{19} of $Sc_2C_2@C_{68}$, and parts c and d of Figure 4 show those corresponding to S_{22} of $Sc_3N@C_{68}$. It can be concluded that the charge transfers from the embedded molecule Sc_2C_2 to the cage C_{68} make great contribution to $\langle\delta(\omega)\rangle$ at the resonant wavelength of 967 nm for the EMF $Sc_2C_2@C_{68}$ and that the charge transfers from the cage of C_{68} to the embedded molecule Sc_3N make substantial contributions to 2PA at the resonant wavelength of 876 nm for $Sc_3N@C_{68}$. The different mechanisms of charge transfers between the $Sc_2C_2@C_{68}$ and $Sc_3N@C_{68}$ can be illustrated by the electron populations. The charge of isolated $[Sc_2C_2]$ has −2.0e based on the calculation of atomic valence state (Sc +3 and C −4). When it is considered in the EMF $Sc_2C_2@C_{68}$, it has +1.428e from the B3LYP/6-311G**

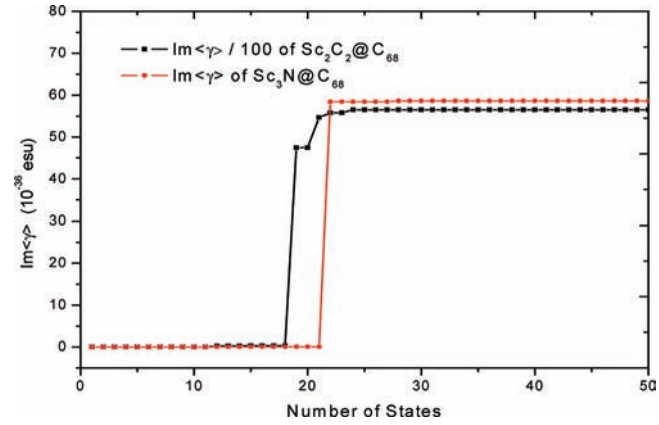

Figure 3. State-dependent imaginary part of third-order polarizability at given wavelength.

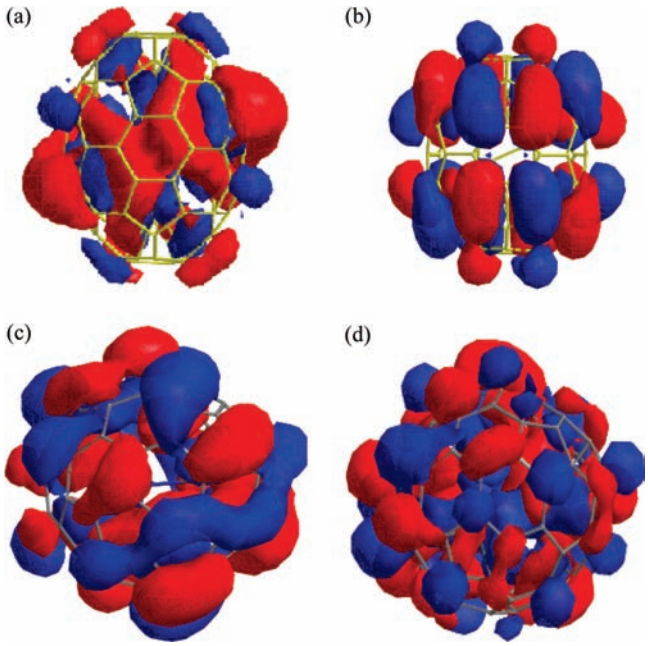

Figure 4. The molecular orbitals involved in the charge transfer processes that make contribution to two-photon absorption cross sections: (a) MO_{223}(HOMO-8) in $Sc_2C_2@C_{68}$; (b) MO_{232} (LUMO) in $Sc_2C_2@C_{68}$; (c) MO_{237} (HOMO-2) in $Sc_3N@C_{68}$; and (d) MO_{245} (LUMO+4) in $Sc_3N@C_{68}$.

calculation (see Tables S3 and S4 in Supporting Information). This implies that the $[Sc_2C_2]$ donates 3.428e to C_{68} after it is embedded into the cage. Using the same analysis procedure, we find that the charges of $[Sc_3N]$ have +6.0e in isolation and +2.665e in the $Sc_3N@C_{68}$, respectively, and that the charge transfers from the cage C_{68} to the Sc_3N are 3.335e within the $Sc_3N@C_{68}$. This result tells us that the increases of π-charges on the cage of C_{68} will result in a larger 2PA cross section in EMFs, which is indicated by $Sc_2C_2@C_{68}$.

2PA is the process in which the energy gap between two real states is bridged by the simultaneous absorption of two photons. Neither photon has enough energy to complete the transition alone. Accordingly, we can think of the first photon as making a virtual transition to a nonexistent intermediate state between the upper and lower levels. In other words, the 2PA state can be constructed by one-electron promotion from ground state to an intermediate state (one-photon state) by absorbing one-photon energy, and then a second promotion from the immediate state to two-photon state by absorbing one-photon energy again. This implies that two-photon resonant transition can be described by three-state model. The peak value of two-photon resonant $\delta(\omega)$ can be represented by $\delta_{g\rightarrow t} \propto (M_{go}^2 M_{ot}^2)/(E_o - E_g - \hbar\omega)^2\Gamma$, where the subscripts g, o, and t refer to ground state, one-photon, and two-photon states, respectively, and $\hbar\omega = (E_t - E_g)/2$. It shows that the $\delta(\omega)$ value increases with products of transition moment $(M^2_{go}M^2_{ot})$ and it increases when the one-photon detuning term $(E_o - E_g - \hbar\omega)$ decreases. Table 2 lists the states involved in 2PA processes and the transition moments from ground-state to one-photon state and from the one-photon state to two-photon states. It also contains the corresponding transition energies and incident photon energies. It can be found from Table 2 that $Sc_3N@C_{68}$ has smaller transition-moment products and larger detuning terms compared with $Sc_2C_2@C_{68}$. This approach provides a direct view of the reason why the 2PA cross section of $Sc_2C_2@C_{68}$ is larger than that of $Sc_3N@C_{68}$.

TABLE 2: The Transition Moments and Energies between the One-Photon States

fullerenes	state→ state	moment (a.u.)	$(M_{go}^2 M_{ot}^2)$	energy (eV)	$\hbar\omega$ (eV)	detuning energy (eV)
$Sc_2C_2@C_{68}$	G → 4	1.1236		1.6846	1.2823	0.4053
	4 → 19	1.6459	3.4200			
	G → 19			2.5587		
$Sc_3N@C_{68}$	G → 2	0.1664		1.8972	1.4158	0.4814
	2 → 22	0.8241	0.0188			
	G → 22			2.8316		

3.3. Three-Photon Absorption. Three-photon absorption (3PA) is cubic-dependent on incident-light intensity, and it may be superior to 2PA in the penetration depth of the excitation volume. Accordingly, 3PA affords the possibility of using a much longer excitation wavelength. Figure 5 shows the plots of wavelength-dependent 3PA cross sections of $Sc_2C_2@C_{68}$ and $Sc_3N@C_{68}$. The peak value of 3PA cross section σ from the circular light polarization is larger than that from linear light polarization. Hereafter, we only consider the 3PA properties of the average linear light-polarization. The peaks of 3PA cross sections are located at the wavelengths of 1264 and 1110 nm for $Sc_2C_2@C_{68}$ and $Sc_3N@C_{68}$, respectively. The peak position of $Sc_2C_2@C_{68}$ is still red-shifted as compared with that of $Sc_3N@C_{68}$. The largest 3PA cross section $\langle\sigma\rangle$ (114.4×10^{-80} cm^6 s^2) of $Sc_2C_2@C_{68}$ at linear polarization is much larger than that (5.95×10^{-80} cm^6 s^2) of $Sc_3N@C_{68}$. The phenomenon can

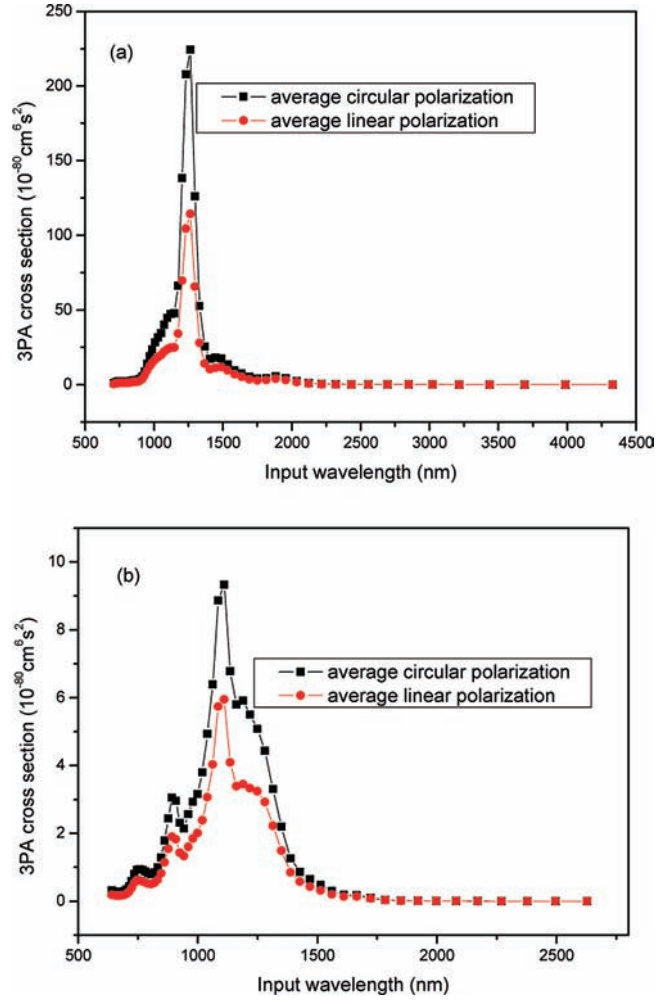

Figure 5. The calculated wavelength-dependent 3PA cross section of (a) $Sc_2C_2@C_{68}$ and (b) $Sc_3N@C_{68}$.

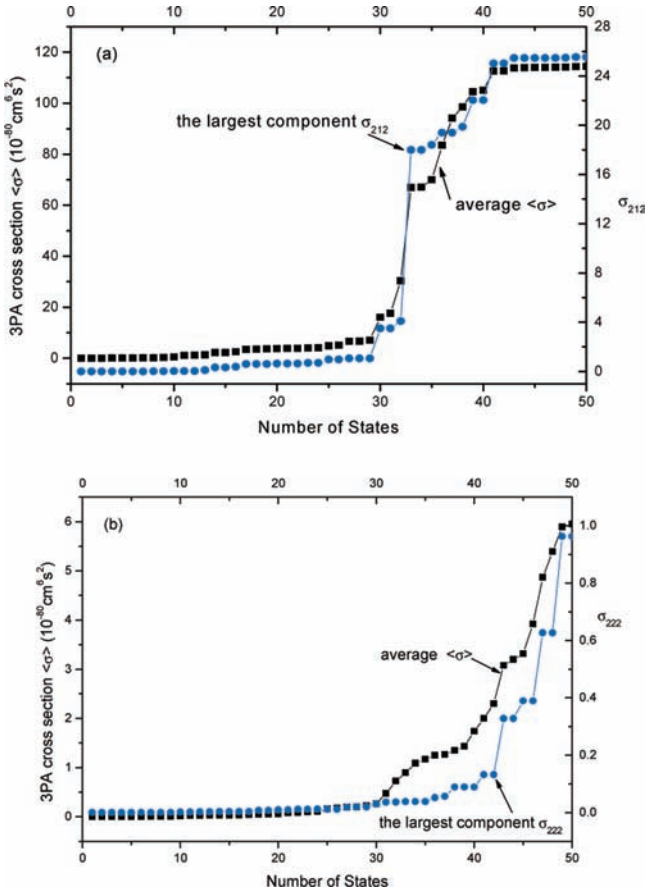

Figure 6. The state-dependent 3PA cross sections of (a) $Sc_2C_2@C_{68}$ at the wavelength of 1264 nm and (b) $Sc_3N@C_{68}$ at the wavelength of 1110 nm.

be understood from the state-dependent 3PA cross section at the given wavelengths of 1264 and 1110 nm for $Sc_2C_2@C_{68}$ and $Sc_3N@C_{68}$, respectively. Figure 6 gives the plots of 3PA cross section $\langle\sigma(\omega)\rangle$ and its largest component vs state numbers at the characteristic wavelength. It shows that S_{33} of $Sc_2C_2@C_{68}$ and S_{43} of $Sc_3N@C_{68}$ make the most contributions to $\langle\sigma(\omega)\rangle$ values at the given wavelength, respectively. S_{33} of $Sc_2C_2@C_{68}$ is mainly constructed by the configuration of $0.3946(MO_{226} \rightarrow MO_{233}) + 0.3802(MO_{227} \rightarrow MO_{234})$. The occupied molecular orbitals of MO_{226} and MO_{227} consist of contributions from the C_{68} cage by 97% and 98%, while the unoccupied molecular orbitals of MO_{233} and MO_{234} both contain contributions from the cage by about 97%. For the $Sc_3N@C_{68}$, S_{43} is mostly constructed by the configuration of $-0.3539(MO_{234} \rightarrow MO_{243}) + 0.3540(MO_{235} \rightarrow MO_{242})$, in which the occupied molecular orbitals of both MO_{234} and MO_{235} contain contributions from the C_{68} cage by 96%, while the unoccupied molecular orbitals of both MO_{242} and MO_{243} contain contributions from the cage by 91%. Therefore it can be found that the charge transfers within the cage C_{68} make a great contribution to $\langle\sigma(\omega)\rangle$ at the peak position of wavelength of 1264 nm for the EMF $Sc_2C_2@C_{68}$, while some charge transfers from the cage of C_{68} to the embedded cluster Sc_3N make the substantial contributions to 3PA at the wavelength of 1110 nm for the $Sc_3N@C_{68}$. This result tells us that the decreases of π-charges on the cage will result in a smaller 3PA cross section in EMFs.

4. Conclusions

Time-dependent density functional theory combined with sum-overstate formula has been employed to model the two- and three-photon absorptions of EMFs $Sc_2C_2@C_{68}$ and $Sc_3N@C_{68}$. The applicability of the calculation method has been tested by comparing the calculated and experimental multiphoton absorptions of *trans*-4, 4′-bis[diphenylamino]stilbene. The electronic origin of multiphoton absorptions (2PA and 3PA) has been identified in view of the state-dependent multiphoton absorption cross sections and the molecular orbitals involved in the charge transfer processes. It is found that the increases of π-charges on the cage of C_{68} will lead to a larger multiphoton absorption cross section in EMFs. Analysis of the three-state model shows that a large two-photon absorption cross section of $Sc_2C_2@C_{68}$ arises from large transition moments and small transition energy as compared with those of $Sc_3N@C_{68}$. The further analysis from molecular orbitals confirms that the charge transfers from the embedded cluster Sc_2C_2 to the cage of C_{68} result in a large two-photon absorption for the $Sc_2C_2@C_{68}$. On the contrary, the charge transfers from the cage of C_{68} to the embedded cluster Sc_3N result in a small two-photon absorption for the $Sc_3N@C_{68}$. The study on the 3PA cross sections of the two species complements this conclusion.

Acknowledgment. This work is supported by the National Natural Science Foundation of China under project 20773131, and the National Basic Research Program of China (No. 2007CB815307), the Science Foundation of the Fujian Province (No. E0210028), and the Funds of Chinese Academy of Sciences (KJCX2-YW-H01). Here we would like to thank Dr. Habenicht in Department of Chemical and Biomolecular Engineering, University of Tennessee, for helping review the paper.

Supporting Information Available: The wavelength-dependent 2PA and 3PA cross sections of tested molecule BDPAS, dipole moments of ground and excitation states and transition moments, and Mulliken populations for $Sc_2C_2@C_{68}$ and $Sc_3N@C_{68}$ EMFs. This material is available free of charge via the Internet at http://pubs.acs.org.

References and Notes

(1) Kim, H. M.; Lee, Y. O.; Lim, C. S.; Kim, J. S.; Cho, B. R. *J. Org. Chem.* **2008**, *73*, 5127.

(2) Fu, J.; Padilha, L. A.; Hagan, D. J.; Van Stryland, E. W.; Przhonska, O. V.; Bondar, M. V.; Slominsky, Y. L.; Kachkovski, A. D. *J. Opt. Soc. Am. B* **2007**, *24*, 56.

(3) Mik, Egbert, G.; van Leeuwen, T. G.; Raat, N. J.; Ince, C. *J. Appl. Physiol.* **2004**, *97*, 1962.

(4) Pirrung, M. C.; Pieper, W. H.; Kaliappan, K. P.; Dhananjeyan, M. R. *Proc. Natl. Acad. Sci. U.S.A.* **2003**, *100*, 12548.

(5) Walker, E.; Dvornikov, A.; Coblentz, K.; Esener, S.; Rentzepis, P. *Opt. Express* **2007**, *15*, 12264.

(6) Kawata, S.; Kawata, Y. *Chem. Rev* **2000**, *100*, 1777.

(7) Denk, W.; Strickler, J.; Webb, W. *Science* **1990**, *248*, 73.

(8) Helmchen, F.; Denk, W. *Nat. Methods* **2005**, *2*, 932.

(9) Sehoon, K.; Heng, H.; Haridas, E. P.; Yiping, C.; Paras, N. P. *Chem. Mater.* **2007**, *19*, 5650.

(10) Capella, M. A. M.; Capella, L. S. *J. Biomed. Sci.* **2003**, *10*, 361.

(11) Shinohara, H. *Rep. Prog. Phys.* **2000**, *63*, 843.

(12) Zhuo, G.; Wang, X.; Wang, D.; Wang, C.; Zhao, X.; Shao, Z.; Jiang, M. *Opt. Laser Technol.* **2001**, *33*, 209.

(13) Kevin, D. B.; Mykhailo, V. B.; Florencio, E. H.; Olga, V. P. *J. Phys. Chem. C* **2008**, *112*, 5618.

(14) Fatouros, P. P.; Corwin, F. D.; Chen, Z.-J.; Broaddus, W. C.; Tatum, J. L.; Kettenmann, B.; Ge, Z.; Gibson, H. W.; Russ, J. L.; Leonard, A. P.; Duchamp, J. C.; Dorn, H. C. *Radiology* **2006**, *240*, 756.

(15) Kato, H.; Kanazawa, Y.; Okumura, M.; Taninaka, A.; Yokawa, T.; Shinohara, H. *J. Am. Chem. Soc.* **2003**, *125*, 4391.

(16) Bolskar, R. D.; Benedetto, A. F.; Husebo, L. O.; Price, R. E.; Jackson, E. F.; Wallace, S.; Wilson, L. J.; Alford, J. M. *J. Am. Chem. Soc.* **2003**, *125*, 5471.

(17) Shi, Z. Q.; Wu, X.; Wang, C. R.; Lu, X.; Shinohara, H. *Angew. Chem., Int. Ed.* **2006**, *45*, 2107.

(18) Olmstead, M. M.; Lee, H. M.; Duchamp, J. C.; Stevenson, S.; Marciu, D.; Dorn, Harry, C.; Balch, A. L. *Angew. Chem., Int. Ed.* **2003**, *42*, 900.
(19) Kato, H.; Taninaka, A.; Sugai, T.; Shinohara, H. *J. Am. Chem. Soc.* **2003**, *125*, 7782.
(20) Maroulis, G.; Begué, D.; Pouchan, C. *J. Chem. Phys.* **2003**, *19*, 794.
(21) Karamanis, P.; Pouchan, C.; Maroulis, G. *Phys. Rev. A* **2008**, *77*, 013201.
(22) Krishnan, R.; Binkley, J. S.; Seeger, R.; Pople, J. A. *J. Chem. Phys.* **1980**, *72*, 650.
(23) Frisch, M. J.; Trucks, G. W.; Schlegel, H. B.; Scuseria, G. E.; Robb, M. A.; Cheeseman, J. R.; Montgomery; J. A. Jr.; Vreven, T.; Kudin, K. N.; Burant; J. C.; Millam, J. M.; Iyengar, S. S.; Tomasi, J.; Barone, V.; Mennucci, B.; Cossi, M.; Scalmani, G.; Rega, N.; Petersson, G. A.; Nakatsuji, H.; Hada, M.; Ehara, M.; Toyota, K.; Fukuda, R.; Hasegawa, J.; Ishida, M.; Nakajima, T.; Honda, Y.; Kitao, O.; Nakai, H.; Klene, M.; Li, X.; Knox, J. E.; Hratchian, H. P.; Cross, V.; Adamo, C.; Jaramillo, J.; Gomperts, R.; Stratmann, R. E.; Yazyev, O.; Austin, A. J.; Cammi, R.; Pomelli, C.; Ochterski, J. W.; Ayala, P. Y.; Morokuma, K.; Voth, G. A.; Salvador, P.; Dannenberg, J. J.; Zakrzewski, V. G.; Dapprich, S.; Daniels, A. D.; Strain, M. C.; Farkas, O.; Malick, D. K.; Rabuck, A. D.; Raghavachari, K.; Foresman, J. B.; Ortiz, J. V.; Cui, Q.; Baboul, A. G.; Clifford, S.; Cioslowski, J.; Stefanov, B. B.; Liu, G.; Liashenko, A.; Piskorz, P.; Komaromi, I.; Martin, R. L.; Fox, D. J.; Keith, T.; Al-Laham, M. A.; Peng, C. Y.; Nanayakkara, A.; Challacombe, M.; Gill, P. M. W.; Johnson, B.; Chen, W.; Wong, M. W.; Gonzalez, C.; Pople, J. A. *Gaussian 03, Revision B.04*; Gaussian, Inc.: Pittsburgh, PA, 2003.
(24) Cheng, W.-D.; Wu, D.-S.; Li, X.-D.; Lan, Y.-Z.; Zhang, H.; Chen, D.-G.; Gong, Y.-J.; Zhang, Y.-C.; Li, F.-F.; Shen, J.; Kan, Z.-G. *Phys. Rev. B* **2004**, *70*, 155401.
(25) Shen, J.; Cheng, W.-D.; Wu, D.-S.; Lan, Y.-Z.; Li, F.-F.; Huang, S.-P.; Zhang, H.; Gong, Y.-J. *J. Phys. Chem. A* **2006**, *110*, 10330.
(26) Orr, B. J.; Ward, J. F. *Mol. Phys.* **1971**, *20*, 513.
(27) Pierce, B. M. *J. Chem. Phys.* **1989**, *91*, 791.
(28) Wu, D.-S.; Cheng, W.-D.; Li, X.-D.; Lan, Y.-Z.; Chen, D.-G.; Zhang, Y.-C.; Zhang, H.; Gong, Y.-J. *J. Phys. Chem. A* **2004**, *108*, 1837.
(29) Cheng, W.-D.; Wu, D.-S.; Zhang, H.; Li, X.-D.; Lan, Y.-Z.; Chen, D.-G.; Wang, H.-X. *J. Chem. Phys.* **2003**, *119*, 13100.
(30) Bredas, J. L.; Adant, C.; Tackx, P.; Persoons, A.; Pierce, B. M. *Chem. Rev.* **1994**, *94*, 243.
(31) Cronstrand, P.; Luo, Y.; Norman, P.; Ågren, H. *Chem. Phys. Lett.* **2003**, *375*, 233.
(32) Cronstrand, P.; Jansik, B.; Jonsson, D.; Luoa, Y.; Ågren, H. *J. Chem. Phys.* **2004**, *121*, 9239.
(33) Zhu, L.; Yang, X.; Yi, Y.; Xuan, P.; Shuai, Z.; Chen, D.; Zojer, E.; Bre'das, J. L.; Beljonne, D. *J. Chem. Phys.* **2004**, *121*, 11060.
(34) Lin, N.; Zhao, X.; Yang, J. X.; Jiang, M. H.; Liu, J. C.; Wang, C. K.; Shi, W.; Meng, J.; Weng, J. *J. Chem. Phys.* **2006**, *124*, 024704.
(35) McClain, W. M. *J. Chem. Phys.* **1971**, *55*, 2789.
(36) Becke, A. D. *J. Chem. Phys.* **1993**, *98*, 5648.
(37) Bauemschmitt, R.; Ahlrichs, R. *Chem. Phys. Lett.* **1996**, *256*, 454.
(38) Casida, M. E.; Jamorski, C.; Casida, K. C.; Salahub, D. R. *J. Chem. Phys.* **1998**, *108*, 4439.
(39) Rumi, M.; Ehrlich, J. E.; Heikal, A. A.; Perry, J. W.; Barlow, S.; Hu, Z.; McCord-Maughon, D.; Parker, T. C.; Ro1ckel, H.; Thayumanavan, S.; Marder, S. R.; Beljonne, D.; Bre'das, J.-L. *J. Am. Chem. Soc.* **2000**, *122*, 9500.
(40) Drobizhev, M.; Karotki, A.; Dzenis, Y.; Aleksander Rebane, A.; Suo, Z.; Spangler, C. W. *J. Phys. Chem. B* **2003**, *107*, 7540.
(41) Drobizhev, M.; Karotki, A.; Kruk, M.; Dzenis, Y.; Rebane, A.; Suo, Z.; Spangler, C. W. *J. Phys. Chem. B* **2004**, *108*, 4221.
(42) Drobizhev, M.; Rebane, A.; Suoc, Z.; Spangler, C. W. *J. Lumin.* **2005**, *111*, 291.
(43) Salek, P.; Ågren, H.; Baev, A.; Prasad, P. N. *J. Phys. Chem. A* **2005**, *109*, 11037.
(44) Reveles, J. U.; Heine, T.; Andreas, M. K. *J. Phys. Chem. A* **2005**, *109*, 7068.

JP810806B